Effects of the interaction range on structural phases of flexible polymers

J. Gross, T. Neuhaus, T. Vogel, and M. Bachmann

Citation: The Journal of Chemical Physics **138**, 074905 (2013); doi: 10.1063/1.4790615
View online: http://dx.doi.org/10.1063/1.4790615
View Table of Contents: http://scitation.aip.org/content/aip/journal/jcp/138/7?ver=pdfcov
Published by the AIP Publishing

Effects of the interaction range on structural phases of flexible polymers

J. Gross,[1,a)] T. Neuhaus,[2,b)] T. Vogel,[1,c)] and M. Bachmann[1,d)]
[1]*Center for Simulational Physics, The University of Georgia, Athens, Georgia 30602, USA*
[2]*Jülich Supercomputing Centre, Forschungszentrum Jülich, D-52425 Jülich, Germany*

(Received 26 November 2012; accepted 23 January 2013; published online 20 February 2013)

We systematically investigate how the range of interaction between non-bonded monomers influences the formation of structural phases of elastic, flexible polymers. Massively parallel replica-exchange simulations of a generic, coarse-grained model, performed partly on graphics processing units and in multiple-Gaussian modified ensembles, pave the way for the construction of the structural phase diagram, parametrized by interaction range and temperature. Conformational transitions between gas-like, liquid, and diverse solid (pseudo) phases are identified by microcanonical statistical inflection-point analysis. We find evidence for finite-size effects that cause the crossover of "collapse" and "freezing" transitions for very short interaction ranges. © *2013 American Institute of Physics*. [http://dx.doi.org/10.1063/1.4790615]

I. INTRODUCTION

The necessity for a better understanding of dynamical and structural properties of polymers has initiated many directions of interdisciplinary research, because structure and function of biopolymers and synthetic variants govern biological processes and technological applications. Nevertheless, over many decades, most of the scientific work has aimed at macroscopic systems such as single polymers with high polymerization degree or polymer melts. This was mainly due to the fact that on one side the experimental equipment was not capable of revealing finer structural details on smaller scales. On the other hand, the theoretical treatment of even very simple polymer models was only possible in limits, where cooperative effects on mesoscopic scales could be neglected. Only computational methods were found to enable investigations of systems, which are governed by finite-size effects on comparatively small scales. The most striking class of polymers is the set of biologically relevant polymers that, in particular, includes the proteins.

However, also computational approaches have always been restricted by available resources and, therefore, many problems have remained unsolved. In recent years, computer simulations have contributed substantially to a better understanding of phase transitions in general, including thermodynamic transitions in polymer systems which require mutual interaction of non-bonded monomers (such as collapse, aggregation, and adsorption at substrates). Many of these studies were done in the conventional way of thinking that phase transitions only occur in very large systems close to the thermodynamic limit. This brought up the idea of finite-size scaling; a concept which has also successfully been applied to polymer systems.[1,2] However, it has also turned out to be quite difficult to use this approach for transitions based on nucleation processes, where local effects, including competing effects of monomer arrangement inside the nucleus and at the surface govern the whole nucleation process. That means, before crystallization can be perceived as a condensation process on macroscopic scales, the system has to pass a series of "subphase" transitions,[3] which depend on microscopic details and do not necessarily systematically scale with system size. This has been extensively studied for small atomic clusters[4–6] and, more recently, for polymers of finite length.[7–12] The simulation and analysis of such transitions is demanding and requires computational methodologies and resources that have only recently become available. These methods, with generalized-ensemble Monte Carlo (MC) algorithms in the lead, even enable a different way of statistical analysis on the basis of the density of states or microcanonical entropy,[13] which, although already having been known since the foundation of statistical mechanics, has widely been neglected in the long period of analytic studies (because the density of states is hardly accessible analytically). A systematic method to analyze structural transitions by means of the inflection points of the inverse microcanonical temperature has been introduced recently.[10]

In this paper, we will investigate how structure formation of a single elastic, flexible polymer depends on the range of mutual interaction between non-bonded monomers. The goal is to construct a phase diagram that separates potential structural phases for all classes of flexible polymers under the influence of a thermal environment. In recent years, much work has been dedicated to the identification of structural phases of flexible polymers by using standard representations of generic coarse-grained lattice and off-lattice models for polymers. However, as recent studies of discrete models have shown,[7,14,15] it is also important to understand to what extent the formation of these structural phases is affected by the effective range of the attractive non-bonded interactions competing with excluded-volume effects. One of the most interesting features found in these studies was that, for sufficiently short interaction range, collapse and nucleation are not

a)gross@physast.uga.edu.
b)t.neuhaus@fz-juelich.de.
c)thomasvogel@physast.uga.edu.
d)bachmann@smsyslab.org. URL: http://www.smsyslab.org.

separate transitions anymore, and a liquid phase does not exist. It is also known that geometric properties of atomic clusters sensitively depend on the range of interaction.[4–6,16]

We present here the results of extensive generalized-ensemble Monte Carlo simulations of a generic Lennard-Jones model for elastic, flexible polymers in continuum in order to reveal the interaction-range dependent phase structure under the influence of finite-size effects. Since the latter essentially affects the behavior in the regime where coil-globule and freezing transitions meet, we also thoroughly compare conventional canonical and more detailed microcanonical analyses of this multiple transition point.

The paper is structured as follows. The flexible polymer model, the multiple-Gaussian modified ensemble replica-exchange Monte Carlo method,[18] and the microcanonical statistical analysis are described in Sec. II. Results including the structural phase diagram are presented in Sec. III. The conclusions of our study are summarized in Sec. IV.

II. MODEL AND METHODS

A. Model

For our study, we employ a generic model of a single elastic, flexible homopolymer chain. The bonds between neighboring monomers are modeled using the anharmonic FENE (finitely extensible nonlinear elastic) potential[19,20]

$$U_{\mathrm{FENE}}(r_{ii+1}) = -\frac{K}{2}R^2 \log\left[1 - \left(\frac{r_{ii+1} - r_0}{R}\right)^2\right]. \quad (1)$$

We locate its minimum at $r_0 = 0.7$, set $R = 0.3$, and choose $K = 40$.[8] In addition to the FENE bonds all monomers, bonded and non-bonded, interact via a truncated, shifted Lennard-Jones potential

$$U_{\mathrm{LJ}}^{\mathrm{mod}}(r_{ij}) = U_{\mathrm{LJ}}(r_{ij}) - U_{\mathrm{LJ}}(r_c), \quad (2)$$

with

$$U_{\mathrm{LJ}}(r_{ij}) = 4\epsilon\left[-\left(\frac{\sigma}{r_{ij} - r_s}\right)^6 + \left(\frac{\sigma}{r_{ij} - r_s}\right)^{12}\right], \quad (3)$$

where the energy and length scales are set to $\epsilon = 1$ and $\sigma = (r_0 - r_s)/2^{1/6}$, respectively. We choose a cut-off radius $r_c = 2.5\sigma + r_s$ such that $U_{\mathrm{LJ}}^{\mathrm{mod}}(r_{ij}) \equiv 0$ for $r_{ij} > r_c$ and $U_{\mathrm{LJ}}(r_c) = (-3\,983\,616/244\,140\,625)\epsilon \approx -0.016317\epsilon$. The total energy of a conformation $\mathcal{C} = (\vec{r}_1, \cdots, \vec{r}_N)$ for a chain with N monomers is then given by

$$E(\mathcal{C}) = \sum_{i<j}^{N} U_{\mathrm{LJ}}^{\mathrm{mod}}(r_{ij}) + \sum_{i}^{N-1} U_{\mathrm{FENE}}(r_{ii+1}). \quad (4)$$

Within our simulations, the parameter r_s is used to control the width of the potential. The qualitative behavior of the influence of r_s on the shape of the potential is shown in Fig. 1. While it is convenient to use r_s in the definition of the potential, it is more useful for the subsequent analysis to introduce the potential width δ as a new parameter. For this purpose

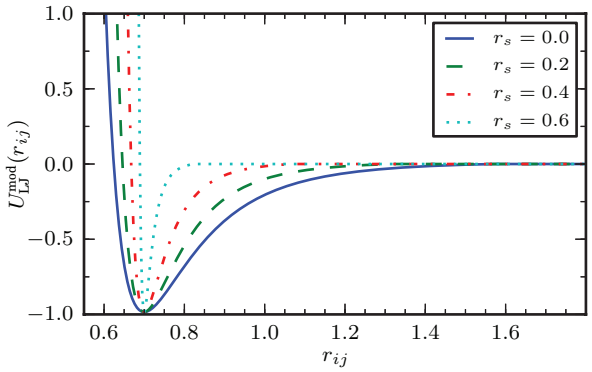

FIG. 1. Behavior of the modified Lennard-Jones potential for different values of r_s.

only, we define a square well potential

$$U_{\mathrm{sq}}(r) = \begin{cases} \infty & \text{if } r \le r_1 \\ -\epsilon_{\mathrm{sq}} & \text{if } r_1 < r < r_2 \\ 0 & \text{if } r \ge r_2 \end{cases}, \quad (5)$$

with the constant $\epsilon_{\mathrm{sq}} = \epsilon/2 + U_{\mathrm{LJ}}(r_c)$ such that $\epsilon_{\mathrm{sq}} = (236\,173\,393/488\,281\,250)\epsilon \approx 0.483683\epsilon$ and r_1 and r_2 being the radii where $U_{\mathrm{LJ}}^{\mathrm{mod}}(r_1) = U_{\mathrm{LJ}}^{\mathrm{mod}}(r_2) = -\epsilon_{\mathrm{sq}}$, independently of r_s (see Fig. 2).

The relationship between the simulation parameter r_s and the potential width δ is linear

$$\delta = r_2 - r_1 = \lambda(r_0 - r_s), \quad (6)$$

with

$$\lambda = 2^{1/6}\left[\left(1 + \sqrt{\frac{1}{2}}\right)^{1/6} - \left(1 - \sqrt{\frac{1}{2}}\right)^{1/6}\right] \approx 0.312382. \quad (7)$$

The maximum value of δ is determined by the unmodified Lennard-Jones term, i.e., for $r_s = 0$, and reads $\delta_{\max} = \lambda r_0 \approx 0.218667$.

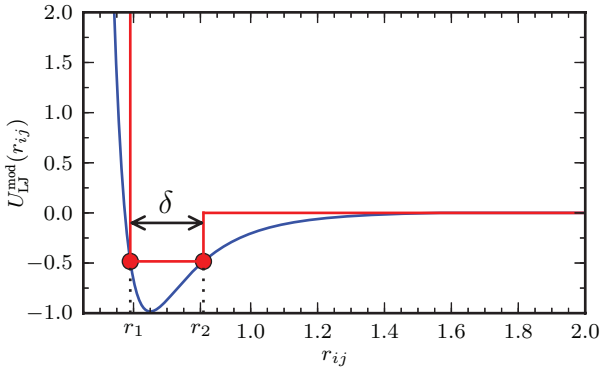

FIG. 2. The potential width δ is defined by the width of a square well potential of depth $-\epsilon_{\mathrm{sq}}$, which is the difference of the two distances r_1 and r_2 where the Lennard-Jones potential equals $-\epsilon_{\mathrm{sq}}$.

B. Simulation method

For our simulations, we employed the replica-exchange Monte Carlo method known as parallel tempering.[22–24] In this method, n_r replicas of the system are simulated at different temperatures. In a single MC update, the conformation of each replica is altered by random local displacements of single monomers. For an inverse thermal energy $\beta = 1/k_BT$, with $k_B \equiv 1$ in our simulations, the probability of accepting such an update is given by the Metropolis criterion[25]

$$p = \min(1, \exp[-\beta(E_{\text{new}} - E_{\text{old}})]), \tag{8}$$

where E_{old} and E_{new} are the energies before and after the proposed update. An exchange of the conformations of replicas i and $i + 1$, with inverse temperatures β_i and β_{i+1}, respectively, is proposed after a fixed number (in this case 1000) of MC steps. This exchange is accepted with the following probability:

$$p = \min(1, \exp[(E_i - E_{i+1})(\beta_i - \beta_{i+1})]). \tag{9}$$

In principle, this method allows each copy of the system to heat up and cool down over the entire simulated temperature range. One set of simulations was performed on graphics processing units (GPUs) using either $n_r = 112$ or 128 replicas. The calculation of the energy was carried out in parallel by using 128 threads per replica. Consequently, there were up to 16 384 threads running concurrently on the graphic cards. The advantages of utilizing graphic cards for parallel tempering simulations of polymers are discussed in more detail in Ref. 17. This simple scheme can be applied for values of δ as small as about 0.06. For smaller values, the freezing transition barrier becomes so strong that an algorithmic improvement is necessary.

Such is made possible by multiple Gaussian modified ensembles (MGME).[18] This Monte Carlo method retains all advantages of parallel tempering, in that it facilitates efficient implementation on parallel computers. At the same time, the sampling of entropically suppressed conformations is increased. The method allows to simulate strong first-order polymer crystallization for chain lengths up to $N = 147$ at very small interaction width $\delta \approx 0.030$ and for the 90-mer down to $\delta \approx 0.015$. A simulation of all structural phases of these polymers with standard parallel tempering is virtually impossible. We performed MGME simulations on a parallel computer cluster using the message passing interface (MPI).

The basic idea of MGME simulations is to multiply the Boltzmann factor of single canonical ensemble by a Gaussian form centered around some central energy value $E_{G,i}$ and a width ΔE_G, such that $P^{\text{B}}_{\text{MGME},i} \sim e^{-\beta_i E - [(E - E_{G,i})/\Delta E_G]^2}$. In consequence, the probability for a state with energy E to occur in the ith modified ensemble becomes

$$P_{\text{MGME},i}(E) \sim e^{S(E) - \beta_i E - \left[(E - E_{G,i})/(\Delta E_G)\right]^2}, \tag{10}$$

where $S(E) = \ln g(E)$ is the microcanonical entropy and $g(E)$ is the density of states. In case of first-order-like transitions, $S(E)$ becomes convex with $d^2S(E)/d^2E > 0$ in a certain finite energy interval, limited by two distinct energies E_+ and E_- with $d^2S(E)/dE^2(E = E_+) = d^2S(E)/dE^2(E = E_-) = 0$. In this case, the energy distribution is bimodal. In MGME simulations, the counter term to $S(E)$ in Eq. (10) of the form $-(E/\Delta E_G)^2$ shifts positive $d^2S(E)/d^2E$ values to negative, provided that ΔE_G is small enough. Thus, energy distribution functions within the single Gaussian ensembles $P_{\text{MGME},i}(E)$ have strictly unimodal shape. This absence of double-peaked distributions improves the Monte Carlo sampling problem of entropically suppressed regions of state space, while a proper choice of the remaining parameters $E_{G,i}$ and β_i ensures a sufficient overlap between neighboring parallel tempering partitions at i and $i + 1$. Possible algorithmic approaches to the parameter choice are described in Ref. 18. For illustration, in Fig. 3 we show a combined energy histogram obtained in actual MGME simulations, the multi-histogram

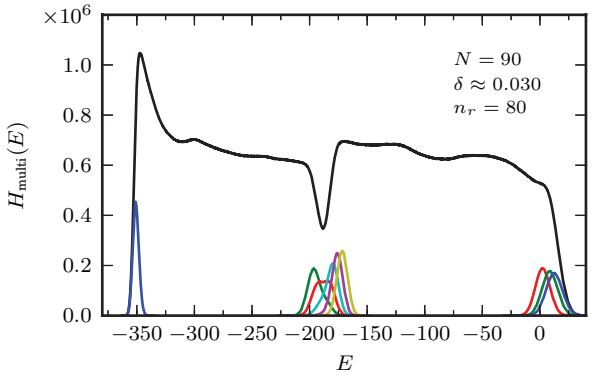

FIG. 3. Accumulated multi-histogram $H_{\text{multi}}(E)$ from MGME simulations for $N = 90$ and $\delta \approx 0.030$ (upper curve). The parallel tempering partition consists of $n_r = 80$ single Gaussian ensembles (replicas). Some histograms for single Gaussian ensemble are also displayed. They are all of unimodal shape.

$$H_{\text{multi}}(E) = \sum_{i=1}^{n_r} H_{\text{MGME,i}}(E), \tag{11}$$

where $H_{\text{MGME,i}}$ is a single histogram in the MGME. The simulation covers the entire energy interval of interest for a $N = 90$ polymer at $\delta \approx 0.030$. In addition, neighboring single energy histograms in-between i and $i + 1$, as displayed in the figure, have sufficiently large overlap to facilitate swap-updates with reasonable acceptance rates. For the given example, the overlap $O_i = \int \min[P_{\text{MGME,i}}(E), P_{\text{MGME,i+1}}(E)]dE$ in-between neighboring probability distributions of the parallel tempering partition was tuned to a value $O_i \approx 0.6\ \forall i$. This particular value results in acceptance rates $P_{\text{acc}} \approx 0.5$ for swap updates. We remark that less optimal parallel tempering partitions for MGME simulations can easily be found, and as long as $O_i > 0.1$ are still considered to be efficient. In our early simulations, we actually employed the simple displacement updates for all Cartesian monomer coordinates. For these, we measure the tunneling auto-correlation time τ_{tunnel} in units of sweeps, which counts the time in-between the assignment of a specific conformation (on the parallel tempering partition) to $i = 1$, then to $i = n_r$ and finally to $i = 1$ again. Figure 4 displays these times (triangles) for the $N = 90$ polymer as a function of δ. We observe rapidly increasing values for short ranged potentials, which renders simulations of short ranged potentials hard. In typical parallel tempering simulations, we perform $\mathcal{O}(10^9)$ sweeps for each of the

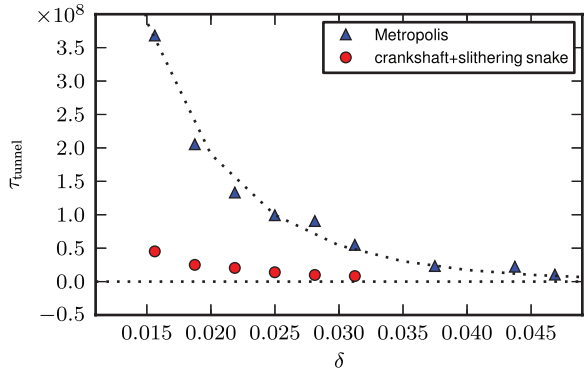

FIG. 4. Tunneling auto-correlation time as explained in the text as a function of δ at $N = 90$ for simple displacement updates (triangles), improved by slithering snake and crankshaft moves (circles). Dotted lines are guides to the eye to illustrate the exponential decay of the tunneling time.

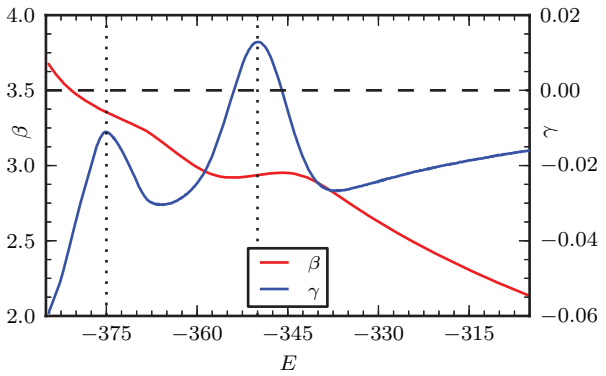

FIG. 5. Comparison of transition signals in β and γ. The peak in $\gamma(E)$ at $E \approx -350$ corresponds to a first-order-like transition. Another peak in γ at $E \approx -375$ marks a second-order-like transition. Both transitions show up as inflection points in $\beta(E)$ at the respective energies. If the peak value of $\gamma(E)$ for a given transition is positive, we classify the transition as of "first order." In line with this, a "second-order" transition is classified by a negative value for the γ-peak.

n_r copies. Including slithering snake and crankshaft updates (circles) reduces the time scale substantially.

C. Microcanonical analysis

For the microcanonical analysis of our data, we use the inflection-point method proposed in Ref. 10. Since all simulations were done using the parallel tempering method, we obtain the energy histograms $H_i(E)$ $(i = 1, \ldots, n_r)$. Each histogram is an estimate for the density of states $g_i(E) \propto H_i(E) \exp(\beta_i E)$ up to an unknown constant, which is different for each β_i. For the analysis of the microcanonical entropy and its derivatives, it is convenient to continue working with the ratio $g_i(E + \Delta E)/g_i(E)$. Entropic differences can then be written as[21]

$$\begin{aligned} \Delta S_i(E) &= S_i(E + \Delta E) - S_i(E) \\ &= \ln[g_i(E + \Delta E)/g_i(E)] \\ &= \ln[H_i(E + \Delta E)] - \ln[H_i(E)] + \beta_i E. \end{aligned} \quad (12)$$

Introducing the following weight:

$$w_i(E) = \frac{H_i(E + \Delta E) \cdot H_i(E)}{H_i(E + \Delta E) + H_i(E)}, \quad (13)$$

which is reciprocally proportional to the variance of $\Delta S_i(E)$, yields the weighted average over all histograms

$$\overline{\Delta S}(E) = \frac{\sum_i \Delta S_i(E) w_i(E)}{\sum_i w_i(E)}. \quad (14)$$

This result can be used for an approximation of the inverse microcanonical temperature, defined as

$$\beta(E) \equiv T^{-1}(E) = \left(\frac{dS}{dE}\right)_{N,V} \approx \frac{\overline{\Delta S}(E)}{\Delta E}. \quad (15)$$

Inflection-point analysis of $\beta(E)$[10] allows us not only to locate, but also to classify transitions in the system. In this scheme, a transition is of *first order*, if the derivative of $\beta(E)$ at the inflection point has a positive peak value $\gamma(E) = d\beta(E)/dE > 0$. Consequently, an inflection point with a negative peak value corresponds to a *second-order*-like transition.

In the example illustrated in Fig. 5, $\beta(E)$ has an inflection point at $E \approx -350$ and the corresponding peak in $\gamma(E)$ is positive. The associated transition is, therefore, first-order-like. Another inflection point of $\beta(E)$ is found at $E \approx -375$. The peak in $\gamma(E)$ for this energy is below zero, indicating a second-order-like transition.

III. RESULTS

A. Comparison with previous work and microcanonical interpretation

In a recent study, Taylor *et al.*[15] investigated a flexible homopolymer chain, where the non-bonded monomers interact via a square-well potential with variable width. Constructing a phase diagram as a function of temperature and potential width they identified three phases for sufficiently large interaction ranges: expanded coils for high temperatures and crystalline structures for very low temperatures, separated by a collapsed-globule phase for intermediate temperatures. The collapse transition was found to be pre-emptied by the freezing transition for narrow potentials. While in a canonical analysis approach the signals for the collapse transition vanish, the microcanonical approach is still able to locate the positions of all transitions.

Since the collapse transition point is included in the Maxwell regime of the liquid-solid transition, Taylor *et al.*[15] concluded that what remains is a first-order-like transition from coil to crystal. This argumentation is fully consistent with the assumption that liquid-solid and coil-globule transitions become indistinguishable in the thermodynamic limit. For the continuum model we used in our study, we can clearly confirm these findings. Figure 6 shows how the inflection point associated with the second-order collapse transition enters the Maxwell regime of the liquid-solid transition (dashed lines), if δ is decreased below a threshold value.

However, this argumentation is not sufficiently consequent in light of the microcanonical interpretation of the results obtained for a finite system. First, the Maxwell construction is adapted from the theory of real gases, where it is necessary to get rid of unphysical behavior in the infinite

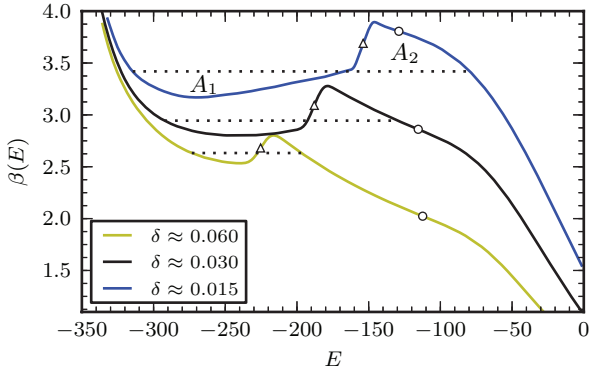

FIG. 6. Comparison of the microcanonical inverse temperature $\beta(E)$ for three values of δ. The triangles mark the corresponding peak position in the derivative of $\beta(E)$ for the freezing transition. The circles correspond to the maxima in $\gamma(E)$ marking the collapse transition. The dotted lines are located at β-values obtained by Maxwell constructions. Areas A_1 and A_2 enclosed by β curves and Maxwell line coincide.

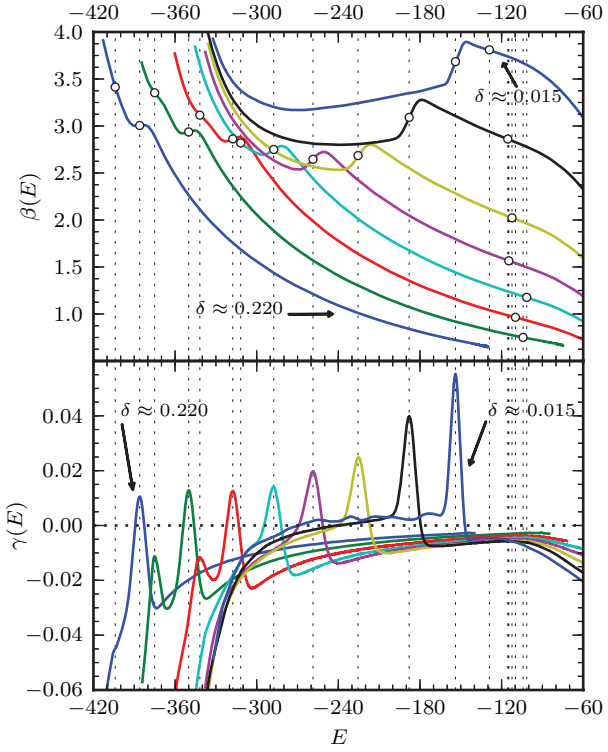

FIG. 7. (Top) The microcanonical inverse temperature as a function of energy for the 90-mer at different values for the potential width δ. All inflection points of the inverse temperature are marked by a circle. (Bottom) Derivative of the inverse temperature $\beta(E)$ as a function of energy.

system. Here, this is not necessary. The "back-bending effect" smoothly disappears for large systems. Therefore, a Maxwell construction is not needed at all. The analysis of inflection points is sufficient to uniquely identify and classify transitions. Second, in contrast to the canonical "heat bath" temperature, the inverse microcanonical temperature is a well-defined quantity on fundamental statistical grounds. Taking this into account, both transitions remain separate, but microcanonically they cross over. This is a pure finite-size effect. Both transition temperatures will converge to the same transition point in the thermodynamic limit.

In Fig. 6, the microcanonical temperature curves are shown for three potential widths, $\delta \approx 0.06$, 0.03, and 0.015. Circles mark the transition points for the Θ-collapse and triangles the freezing transition. In addition to the results from the inflection-point analysis, the Maxwell line associated with the freezing transition is also included. While for rather broad potentials, i.e., $\delta \gtrsim 0.1$ the temperatures obtained by inflection-point analysis and Maxwell construction match, these definitions of the transition temperature differ for narrower potentials.

B. δ dependency

In the following, we will investigate how the interaction range δ of the potential influences transition points in the system. We have plotted the first and second derivatives of the microcanonical entropy for the 90-mer in Fig. 7 as well as specific heat curves and thermal fluctuations of the radius of gyration in Fig. 8. In Fig. 7 (top), the inverse microcanonical temperature is shown as a function of energy. The unmodified and largest interaction range $\delta = \delta_{\max} \approx 0.22$ corresponds to the leftmost temperature curve. Two effects can be observed as the potential width δ is reduced: The freezing transition marked by the non-monotonic region, also referred to as "back-bending" or "convex intruder,"[13] is shifted to higher energies. It also gets more pronounced for narrower potentials. Another effect of narrowing the interaction length is that the collapse transition, indicated by the shoulders in the curves, shifts to lower temperatures. The difference in transition temperatures becomes smaller and smaller for shorter interactions range. In the bottom part of Fig. 7, we show the second derivative of the entropy. With decreasing potential width the freezing transition, signaled by the peak of positive value, shifts to higher energies. The first four curves also show a peak with negative value below the freezing transition, marking the solid-solid transition from anti-Mackay to Mackay overlayers in the incomplete outer shell of the icosahedron in the core. Note that the solid-solid transitions are second-order-like and occur only for $\delta > 0.12$. At higher energies, above the freezing transition, the curves exhibit a maximum marking the collapse transition. This maximum is shifted to lower energies, as δ decreases.

We also looked at two canonical quantities to identify transitions in the system. A typical quantity that gives insight into the thermodynamic behavior of the system is the specific heat, as shown in Fig. 8(a). With decreasing potential width, the signal for the freezing transition, i.e., the pronounced peak at low temperatures, shifts to slightly higher temperatures. For smaller values of the interaction length, the freezing temperature drops again. The maxima of the peaks increase with decreasing δ. The solid-solid transition is just visible as a small shoulder below the freezing peak. While the freezing temperature changes only slightly, the collapse temperature undergoes more significant changes. The shoulders indicating the collapse transitions become narrower with decreasing potential width. In this case, it is often more advantageous to investigate structural quantities, such as the radius of

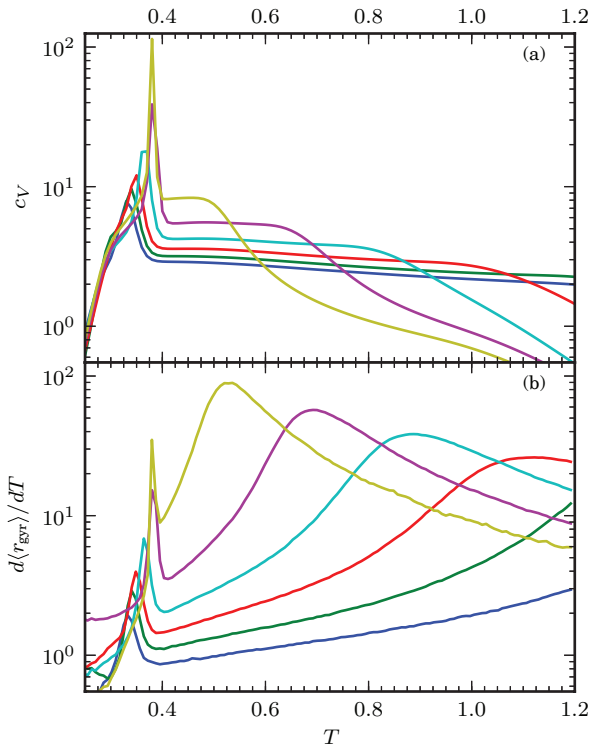

FIG. 8. (a) Specific heat and (b) thermal fluctuation of the radius of gyration for the 90-mer parametrized by δ. The color code for δ is given above in Fig. 7.

gyration r_{gyr}, which is a measure for the spatial extension of the polymer. Let us discuss the thermal fluctuations of r_{gyr} as shown in Fig. 8(b). For each δ, there are two prominent peaks. The low-temperature peaks belong to the liquid-solid transition and their locations agree well with those of the respective specific heat peaks. At higher temperatures, we find very pronounced peaks that indicate the collapse transition. Again, we can see that with smaller δ the difference between gas-liquid and liquid-solid transition temperatures is getting smaller. The Θ-collapse moves to lower temperatures for short interaction ranges. To compare different approaches for transition temperatures, we show the behavior of three definitions for the freezing temperature in Fig. 9. While specific heat peaks and Maxwell construction agree over the entire δ-range, the values obtained via microcanonical analysis visibly deviate for $\delta \lesssim 0.1$. This is not surprising, because in the case of the specific heat and Maxwell indicators freezing and collapse signals mix, whereas the inflection points purely indicate the freezing transition only. Therefore, we will construct the structural phase diagram in the following entirely by means of the microcanonical inflection points of the inverse temperature.

C. Phase diagram

With all the transition temperatures acquired from the microcanonical analysis, we can construct the structural phase diagram for the 90-mer, parametrized by temperature T and interaction range δ. There are three major phases, see Fig. 10. In the "gas" phase **G** at high temperatures and short-range interaction, polymer conformations are dominated by

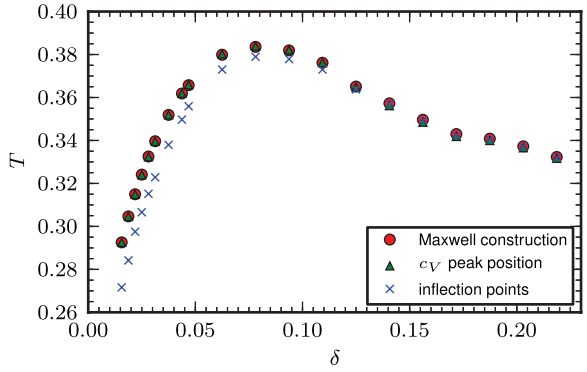

FIG. 9. Comparison of three different definitions for the freezing transition temperature. The crosses are transition temperatures indicated by the respective peaks in the first derivative of the microcanonical entropy. Peak positions of the specific heat are represented by triangles. The circles are the transition points obtained by Maxwell construction.

expanded coils. For interaction ranges $\delta \gtrsim 0.02$, the "liquid" phase **L** separates the gas phase from distinct solid phases. The red curve in Fig. 10 is the Θ-transition line, where the expanded coil collapses into disordered, but compact globular states. Reducing the temperature, the polymer structures change from globular to crystalline at the freezing transition line indicated by the green line. With decreasing potential width the liquid phase region becomes smaller, as the collapse transition shifts to lower temperatures. The inset in Fig. 10 shows the crossover of collapse and freezing at very small interaction ranges. In the microcanonical analysis, it is still possible to single out both transition temperatures. At about $\delta = 0.12$ the solid-solid transition (blue line) merges with the freezing transition. The solid phase $\mathbf{S_{ico-aM}}$ is dominated by structures with at least one icosahedral core and an incomplete outer shell of anti-Mackay type (hcp), see Figs. 1 and 2 in Ref. 8. By reducing the temperature further and passing the solid-solid transition line, the packing is optimized and a Mackay-type fcc layer forms (phase $\mathbf{S_{ico-M}}$). However, the icosahedral interior becomes energetically less optimal for $\delta < 0.15$, and it is replaced by a decahedral arrangement of monomers. These structures can also possess extended fcc-packed fractions ($\mathbf{S_{fcc/deca}}$). Following former studies of atomic cluster models with short-ranged interactions,[4–6] one might expect a separate fcc phase to be present at extremely small δ-values and temperatures. We will discuss this crossover in more detail for a simpler example in the following.

D. Analysis of low-temperature structures

The characterization of the solid phases in the structural phase diagram is challenging and almost completely determined by surface effects. It is instructive to investigate the low-temperature crystal structures of flexible polymers at different ranges δ of the monomer–monomer interaction potential. As an example, we choose the 55-mer, which forms a perfectly shaped icosahedron for $\delta = \delta_{max} \approx 0.220$.[8] In contrast to the 90-mer, its geometric phases are more stable and can be identified clearly. The qualitative behavior however, is similar for longer chains.

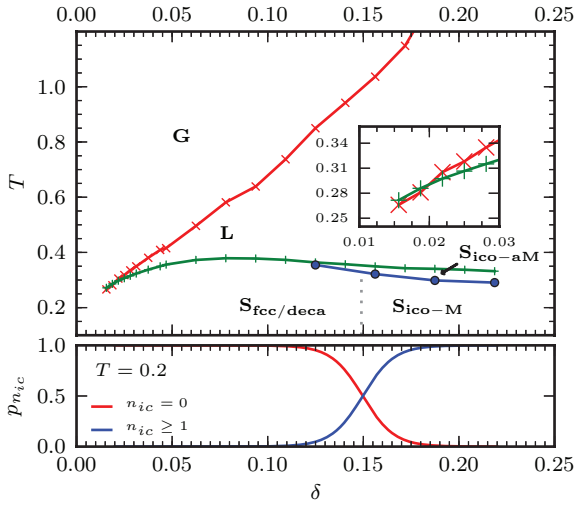

FIG. 10. (Top) Phase diagram for the 90-mer, obtained by pure microcanonical analysis. The inset shows the crossover of the transition temperatures for collapse and freezing transition. (Bottom) Probability for zero ($n_{ic} = 0$) and nonzero ($n_{ic} \geq 1$) number of icosahedral cores in low temperature structures, cf. Ref. 8.

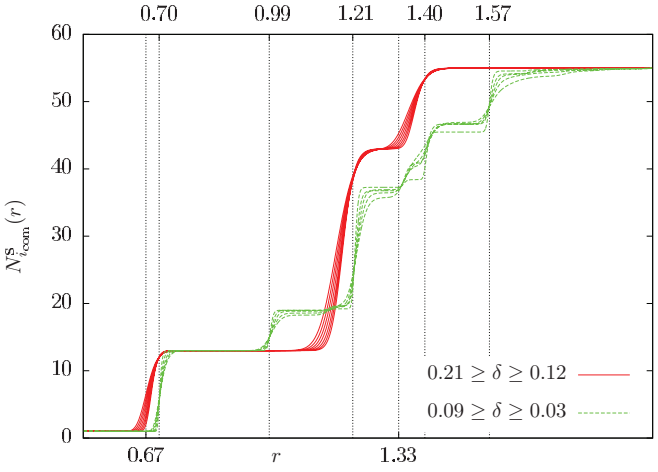

FIG. 11. Averaged integrated radial distribution functions $N^s_{i_{com}}(r)$ for the $N = 55$-mer at different values of δ. Data were obtained from many independent low-energy configurations at inverse microcanonical temperatures $4 \leq \beta \leq 5$. Curves are plotted for different values of δ in steps of $\Delta\delta \approx 0.015$. Grid lines and values at top scale correspond to nth nearest neighbor ($1 \leq n \leq 5$) positions in the fcc-lattice with lattice constant r_0. Grid lines and values at bottom scale correspond to radii of circumscribed spheres of icosahedra with edge lengths r_0 and $2r_0$, cf. Eq. (1).

As a first step, we pick 10^6 independent conformations from the lowest-temperature partition of the multiple Gaussian modified ensemble for every $0.030 \leq \delta \leq 0.220$ in steps of $\Delta\delta \approx 0.015$. The inverse microcanonical temperatures of those conformations are in the range $4 \leq \beta \leq 5$. For the identification of the solid phases, it is useful to measure the integrated radial distribution function with respect to the particle closest to its center of mass (com), i.e., the total number of monomers inside a sphere of radius r around the center monomer i_{com}

$$N^s_{i_{\text{com}}}(r) = \sum_{i \neq i_{\text{com}}} \Theta(r - r_{i,i_{\text{com}}}), \tag{16}$$

where $r_{i,i_{\text{com}}}$ is the distance between monomer i and the center monomer, and $\Theta(r)$ is the Heaviside function. The results are shown in Fig. 11, where each individual curve is the average over the data measured for each of the 10^6 conformations. One can clearly differentiate two types of curves for $N^s_{i_{\text{com}}}(r)$. For $\delta = \delta_{\max} \approx 0.220$, we know that the monomer positions correspond to the vertices in two icosahedral layers with radii of circumscribed spheres of 0.67 and 1.33, containing 13 and 55 monomers, respectively. That fact is clearly supported by the corresponding jumps in $N^s_{i_{\text{com}}}(r)$ marked by grid lines at the bottom scale. For decreasing interaction range, starting at $\delta < 0.12$, the shape of $N^s_{i_{\text{com}}}(r)$ changes qualitatively, indicating that the low-energy states are not icosahedral anymore, which is consistent with Fig. 10 (bottom). The function now shows jumps at radii corresponding to nth nearest neighbor distances in the fcc lattice (upper scale and grid lines). We emphasize that this crossover picture is very stable, even though we measure at temperatures well above $T = 0$.

In order to unravel the structural details, we now look at the putative ground-state structures and measure their (binned) pair distribution function

$$g(r) = \sum_j \left(N^s_j(r + 0.5\Delta r) - N^s_j(r - 0.5\Delta r) \right), \tag{17}$$

where we set $\Delta r \leq 10^{-2}$. In other words, we measure distances between all pairs of monomers in the configuration, rather than only the distance of all monomers from a single center monomer as above, and count them in a histogram. We can clearly differentiate three different structural types in different regions of the interaction length. We plot $g(r)$ in Fig. 12 for three representative values of δ and visualize the corresponding conformations in Fig. 13. The peaks of the red curves (open squares) in Fig. 12 correspond to icosahedral structures, which have been discussed above. For very small δ (blue peaks, filled diamonds), i.e., for very short ranged potentials, we find that all peaks coincide with nearest neighbor positions in the fcc lattice. In Fig. 12, the values at the

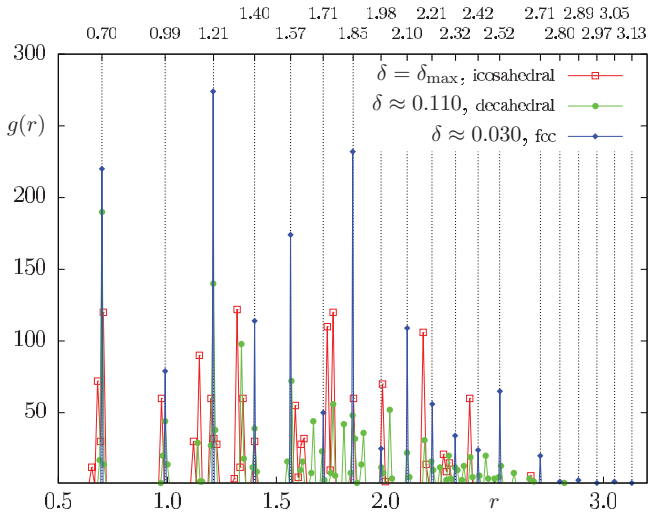

FIG. 12. Pair distribution function for ground states found at $\delta = \delta_{\max}$ (open squares), $\delta \approx 0.110$ (filled circles) and $\delta \approx 0.03$ (filled diamonds). Grid lines and values at top scale correspond to nth nearest neighbor ($1 \leq n \leq 19$) positions in the fcc-lattice with lattice constant r_0, cf. Eq. (1).

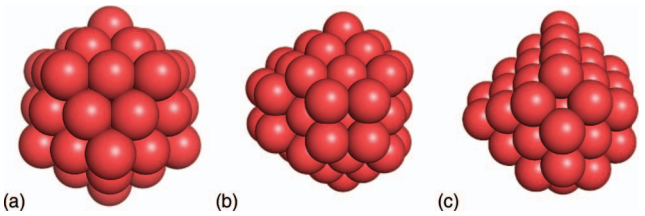

FIG. 13. Visualizations of ground-state structures corresponding to data plotted in Fig. 12. (a) Icosahedron at $\delta = \delta_{\max}$, cf. Ref. 8; (b) $\delta \approx 0.110$, cf. decahedral structure 55C in Ref. 5; (c) $\delta \approx 0.030$, all monomers occupy atomic positions at the fcc lattice.

top scale and the grid lines correspond to the nth-to-nearest neighbor distances ($1 \leq n \leq 19$) in the fcc lattice. All peaks of $g(r)$ of the ground state at $\delta \approx 0.030$ agree very well with these values. However, there are structures in-between (green peaks, filled squares), which are neither icosahedral nor completely fcc structures. Those structures resemble ground states found for atomic, range-dependent Morse clusters.[4,5] In fact, the ground state at $\delta = 0.110$ corresponds to the decahedral structure "55C" found in Ref. 5 (cf. Fig. 13 (b) and Fig. 7 in Ref. 5). For other values of δ close to 0.110, we also find the defective decahedral structures described there.

IV. SUMMARY

We have studied the influence of the interaction length of a Lennard-Jones potential on the structural behavior of an elastic flexible polymer. We applied advanced simulation methods by using replica-exchange parallel tempering on graphics cards and multiple Gaussian modified ensembles to tackle the strong first-order-like behavior of the freezing transition. We employed the microcanonical inflection-point analysis method[10] that made it possible to construct a structural phase diagram for an elastic flexible polymer with 90 monomers. This analysis of the microcanonical entropy allows to resolve the positions of structural transitions, which are much more uncertain in canonical analyses. We are able to precisely locate and also classify transitions by investigating the first and second derivative of the entropy. Both derivatives can be evaluated easily. We find that the liquid phase, separating the extended coil "gas"-like phase from the crystalline solid phases, becomes smaller for shorter interaction ranges. For sufficiently small interaction range, we eventually observe a crossover of transition lines. The crossover point marks the triple point in the thermodynamic limit and thus the direct transition from gas to solid. According to the microcanonical signals, both transitions remain separate for finitely long polymers. Summarizing the structural analysis of the solid phases, we find that the icosahedral ground-state structures identified for the standard Lennard-Jones potential[8] do not survive at smaller interaction ranges. In analogy to former studies of atomic Morse clusters,[4–6] we find transitions from icosahedral to decahedral and fcc structures for decreasing interaction range. These transitions are strongly influenced by the repulsive part of the potential as they are mainly triggered by released stresses in the conformation.

ACKNOWLEDGMENTS

This work has been partially supported by the National Science Foundation (NSF) under Grant No. DMR–1207437 and by the supercomputer time grant VSR Project 5082 of the Forschungszentrum Jülich.

[1] P.-G. de Gennes, *Scaling Concepts in Polymer Physics* (Cornell University, Ithaca, 1979).
[2] D. P. Landau and K. Binder, *A Guide to Monte Carlo Simulations in Statistical Physics*, 3rd ed. (Cambridge University Press, New York, 2009).
[3] C. Junghans, M. Bachmann, and W. Janke, Phys. Rev. Lett. **97**, 218103 (2006); C. Junghans, W. Janke, and M. Bachmann, Comput. Phys. Commun. **182**, 1937 (2011).
[4] J. P. K. Doye, D. J. Wales, and R. S. Berry, J. Chem. Phys. **103**, 4234 (1995).
[5] J. P. K. Doye and D. J. Wales, J. Phys. B **29**, 4859 (1996).
[6] L. Cheng and J. Yang, J. Phys. Chem. A **111**, 5287 (2007).
[7] T. Vogel, M. Bachmann, and W. Janke, Phys. Rev. E **76**, 061803 (2007).
[8] S. Schnabel, T. Vogel, M. Bachmann, and W. Janke, Chem. Phys. Lett. **476**, 201 (2009); S. Schnabel, M. Bachmann, and W. Janke, J. Chem. Phys. **131**, 124904 (2009).
[9] D. T. Seaton, T. Wüst, and D. P. Landau, Comput. Phys. Commun. **180**, 587 (2009); Phys. Rev. E **81**, 011802 (2010).
[10] S. Schnabel, D. T. Seaton, D. P. Landau, and M. Bachmann, Phys. Rev. E **84**, 011127 (2011).
[11] T. Vogel, T. Neuhaus, M. Bachmann, and W. Janke, Europhys. Lett. **85**, 10003 (2009).
[12] T. Vogel, T. Neuhaus, M. Bachmann, and W. Janke, Phys. Rev. E **80**, 011802 (2009).
[13] D. H. E. Gross, *Microcanonical Thermodynamics* (World Scientific, Singapore, 2011).
[14] F. Rampf, W. Paul, and K. Binder, Europhys. Lett. **70**, 628 (2005); W. Paul, T. Strauch, F. Rampf, and K. Binder, Phys. Rev. E **75**, 060801(R) (2007).
[15] M. P. Taylor, W. Paul, and K. Binder, J. Chem. Phys. **131**, 114907 (2009); Phys. Rev. E **79**, 050801(R) (2009).
[16] G. A. Vliegenthart, J. F. M. Lodge, and H. N. W. Lekkerkerker, Physica A **263**, 378 (1999).
[17] J. Gross, W. Janke, and M. Bachmann, Comput. Phys. Commun. **182**, 1638 (2011); Phys. Procedia **15**, 29 (2011).
[18] T. Neuhaus and J. S. Hager, Phys. Rev. E **74**, 036702 (2006).
[19] R. B. Bird, C. F. Curtiss, R. C. Armstrong, and O. Hassager, *Dynamics of Polymeric Liquids*, 2nd ed. (Wiley, New York, 1987).
[20] A. Milchev, A. Bhattacharya, and K. Binder, Macromolecules **34**, 1881 (2001).
[21] M. Möddel, M. Bachmann, and W. Janke, Macromolecules **44**, 9013 (2011).
[22] R. H. Swendsen and J.-S. Wang, Phys. Rev. Lett. **57**, 2607 (1986).
[23] C. J. Geyer in *Computing Science and Statistics: Proceedings of the 23rd Symposium on the Interface*, edited by E. M. Keramidas (Interface Foundation, Fairfax, VA, 1991), pp. 156–163.
[24] K. Hukushima and K. Nemoto, J. Phys. Soc. Jpn. **65**, 1604 (1996).
[25] N. Metropolis, A. W. Rosenbluth, M. N. Rosenbluth, A. H. Teller, and E. Teller, J. Chem. Phys. **21**, 1087 (1953).